

## Evolution of a colloidal critical state in an optical pinning potential landscape

Pamela T. Korda,<sup>1</sup> Gabriel C. Spalding,<sup>2</sup> and David G. Grier<sup>1</sup>

<sup>1</sup>*Department of Physics, James Franck Institute, and Institute for Biophysical Dynamics, The University of Chicago, Chicago, Illinois 60637*

<sup>2</sup>*Department of Physics, Illinois Wesleyan University, Bloomington, Illinois 61702*

(Received 11 December 2001; published 26 June 2002)

As a step toward isolating the influence of a modulated substrate potential on dynamics and phase transitions in two dimensions, we have studied the behavior of a monolayer of colloidal spheres driven by hydrodynamic forces into a large array of holographic optical tweezers. These optical traps constitute a substrate potential whose symmetry, separation, and depth of modulation can be varied independently. We describe a particular set of experiments, in which a colloidal monolayer invades the optical pinning potential much as magnetic flux lines invade type II superconductors, including cooperative avalanches, streaming motion, and a symmetry-altering depinning transition. The jammed intermediate state in this process resembles the critical state long associated with flux entering zero-field-cooled superconductors. By tracking the particles' motions, we are able to determine the microscopic processes responsible for the evolution of the colloidal critical state and compare these with recent simulations of flux-line dynamics.

DOI: 10.1103/PhysRevB.66.024504

PACS number(s): 74.60.Ge, 82.70.Dd, 87.80.Cc

In the absence of an externally imposed potential energy landscape, the behavior of two-dimensional systems is wholly determined by interactions among the constituent particles. Examples of such systems include electrons on the surface of liquid helium, vortices in clean type II superconductors, and colloidal monolayers. Colloidal monolayers in particular have been studied as model systems whose phase behavior offers insight into the general mechanisms of structural phase transitions in reduced dimensionality.<sup>1</sup>

In contrast, the majority of two-dimensional systems are strongly influenced by their constituent particles' interactions with substrate potentials. Adatoms adsorbed on crystal surfaces,<sup>2</sup> magnetic flux lines pinned in defected and patterned<sup>3-8</sup> type II superconductors, atoms imbedded into graphite intercalation compounds,<sup>9</sup> and charge density waves<sup>10</sup> all reflect such an influence with the appearance of different thermodynamic, dynamic, and kinetic phases and states.

Understanding how substrates modify two-dimensional phase behavior is complicated in experimental studies by the comparative difficulty of quantifying and controlling substrates' properties. However, colloids' interaction with easily controlled external forces offers some possibilities. For example, a physically textured surface with micrometer-scale features can influence the free energy of a colloidal overlayer, either through electrostatic interactions or through entropic depletion attractions mediated by small dispersed particles.<sup>11</sup>

Alternatively, a pattern of light applied to the sample can create a modulated potential energy landscape with which the colloid can interact.<sup>12-15</sup> We have utilized this approach by applying the holographic optical tweezer technique<sup>16-18</sup> to create tailored optical potential landscapes for colloidal particles. This paper describes experimental observations of convection-driven colloidal transport into a large, initially empty array of discrete holographic optical traps. The resulting behavior is reminiscent of magnetic flux lines' invasion of a zero-field-cooled type II superconductor.

Each potential well in our controlled potential energy landscape is a discrete optical tweezer,<sup>19</sup> a three-dimensional optical trap for dielectric particles formed when an intense beam of light is brought to a diffraction-limited focus by a high numerical aperture lens. Rather than using  $N$  separate beams to produce  $N$  tweezers, we use a computer-designed diffractive optical element<sup>18</sup> (DOE) to modulate the wave front of a single beam so that it reproduces the interference pattern of  $N$  beams all passing through the DOE's plane. A telescope projects the modulated wave front onto the back aperture of a  $100\times$  N.A. 1.4 S-Plan Apo oil immersion objective lens that then focuses the light into an array of optical traps in its focal plane.<sup>16,18</sup> Figure 1 schematically depicts the optical train used in this study.

Applying such an array of optical traps to a low-density

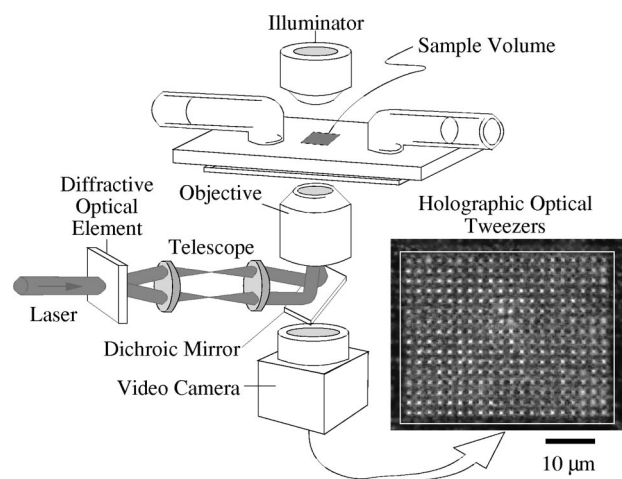


FIG. 1. Schematic diagram of holographic optical tweezer system projecting a  $16\times 20$  array of optical traps into a sample volume containing a colloidal monolayer. The inset is a video micrograph of light from the optical tweezers reflected by the lower glass-water interface. The superimposed rectangle indicates the array's domain in subsequent figures.

colloidal suspension generally causes particles in the immediate neighborhood of traps to become immobilized, and leaves those farther from the array unaffected. In this sense, each trap is analogous to a pinning center for flux lines in a type II superconductor, and thus the holographic optical tweezer array can be considered an “optical pinscape” for colloidal particles.

The samples used in this study consist of silica spheres of radius  $a=0.75 \mu\text{m}$  (Bangs Labs 4258) suspended in deionized water with a total ionic concentration around  $n=10^{-6}$  M. The suspension is confined between two glass plates separated by  $40 \mu\text{m}$ . All parts are cleaned stringently before assembly and flushed copiously with deionized water afterwards to minimize contamination by stray ions. Experiments are performed at an ambient temperature of  $T=295 \pm 1$  K. The sample cell is mounted on the stage of an inverted optical microscope and imaged in bright field onto an attached charge-coupled device (CCD) video camera. The objective lens of the microscope both forms the array of optical tweezers and creates images of the colloid. Images of spheres in a  $(70 \times 55)\text{-}\mu\text{m}^{-2}$  field of view near the center of the sample volume are recorded before being digitized and analyzed with precision particle tracking algorithms.<sup>20</sup> Using these methods, we locate individual spheres’ centroids to within 20 nm in the plane at 0.5-sec intervals.

Because silica’s density of  $2.2 \text{ g/cm}^3$  greatly exceeds that of water, the spheres sediment to the bottom of the sample volume, forming an essentially two-dimensional layer of areal density  $3 \times 10^{-3} \mu\text{m}^{-2}$ . Gravity is opposed by the charged spheres’ electrostatic repulsion from the similarly charged lower glass-water interface. Dissociation of terminal silanol groups endows each sphere with an effective surface charge number of roughly  $Z=5000$  electron equivalents<sup>21,22</sup> and imbues the glass wall with a comparable surface charge density of  $-2000e_0 \mu\text{m}^{-2}$ , where  $e_0$  is the elementary charge.<sup>22</sup> The monolayer achieves equilibrium at a center-to-surface height of about  $h=0.9 \mu\text{m}$ , as determined by optical microscopy.

To such monolayers, we apply an optical pinscape composed of a  $20 \times 16$  square array of traps, with lattice spacing  $1.8 \mu\text{m}$ . The inset of Fig. 1 shows light reflected when the tweezer array is focused on the lower glass-water interface at low intensity. For the experiments, the array is focused  $0.9 \mu\text{m}$  above the lower glass wall and powered by 1.75 W of laser light at 532 nm from a diode-pumped frequency-doubled Nd:YVO<sub>4</sub> laser (Coherent Verdi). Each trap in this array is capable of localizing a single sphere in three dimensions against random thermal forces without appreciably changing the sphere’s height above the wall.

Light from the trap array also impinges on a small region of gold film evaporated onto the upper glass wall. The resulting inhomogeneous local heating drives a toroidal convection roll that spreads out along the upper wall and returns along the bottom. This flow advects spheres along the bottom of the sample cell toward the array of traps from a region extending for hundreds of micrometers in all directions, and at speeds in the range of  $v=7.9 \pm 0.1 \mu\text{m/sec}$  in the field of view. No-flow boundary conditions minimize the flow’s out-of-plane component at the lower wall so that the convection-

driven spheres remain sedimented into a monolayer. Advection towards the pinscape only occurs when the optical traps are illuminated and ceases immediately once they are extinguished.

Before the laser is turned on, the sample is uniformly dilute, with only a few particles in the field of view at any time. When the pinscape is activated and the toroidal flow is established, spheres flow rapidly toward the illuminated region. The first arrivals occupy the perimeter of the tweezer array, impeding flow into the interior. Additional spheres collect outside the array, forming a domain of triangular crystal with a nearest-neighbor separation of  $2.5 \pm 0.1 \mu\text{m}$ . This can be seen in Fig. 2, where the region occupied by the optical pinscape is outlined in white.

The exterior triangular crystal is stabilized by the same hydrodynamic pressure that drives spheres towards the pinscape. Turning off the laser at this point leaves the exterior crystal in an unstable superheated state,<sup>23,24</sup> which melts immediately. This melting process shows no sign of the anomalous long-range attractions<sup>23,24</sup> that have been observed in colloidal interaction measurements on confined polystyrene spheres.<sup>24–27</sup> Instead, it is consistent with recent measurements of screened Coulomb repulsions among similar colloidal silica spheres near a single glass wall under comparable conditions.<sup>21</sup> We expect, therefore, that the spheres in the present experiment also repel each other according to the conventional Derjaguin-Landau-Verwey-Overbeek (DLVO) theory.<sup>21</sup> Thus the electrostatic force between two spheres at center-to-center separation  $r$  has the form<sup>28</sup>

$$F(r) = \frac{Z^2 e_0^2}{\epsilon} \left[ \frac{\exp(-\kappa a)}{1 + \kappa a} \right]^2 \left( \frac{1}{r} + \kappa \right) \frac{\exp(-\kappa r)}{r}, \quad (1)$$

where the Debye screening length  $\kappa^{-1}$  is set by the concentration  $n$  of dissolved ions through  $\kappa^2 = 4\pi e_0^2 n / (\epsilon k_B T)$  in an electrolyte of dielectric constant  $\epsilon$ .

In this case, the Stokes drag<sup>29</sup>

$$F_h = \frac{6\pi\eta a v}{1 + \frac{9}{16} \frac{a}{h} + \frac{1}{8} \left( \frac{a}{h} \right)^3 - \frac{45}{256} \left( \frac{a}{h} \right)^4 - \frac{1}{16} \left( \frac{a}{h} \right)^5} = 0.3 \text{ pN} \quad (2)$$

exerted on each stationary sphere at the edge of the crystal by the flowing water ( $\eta=1$  cP) is balanced by a nearest-neighbor electrostatic repulsion. The observed nearest-neighbor separation of  $r=2.5 \mu\text{m}$  at the surface of the crystal is therefore consistent with a screening length of  $\kappa^{-1} \approx 200$  nm, and thus with the ionic strength of  $n \approx 10^{-6}$  M. These values agree with direct interaction measurements on comparably prepared suspensions.<sup>20,21,30</sup> Similarly, the optical tweezers’ ability to trap spheres at least marginally against both hydrodynamic and nearest-neighbor forces reveals their maximum trapping force to be roughly 0.6 pN.

Figure 2 shows how a typical colloidal monolayer evolves under the combined influence of in-plane hydrodynamic pressure, particle-particle interactions, and the optical pin-

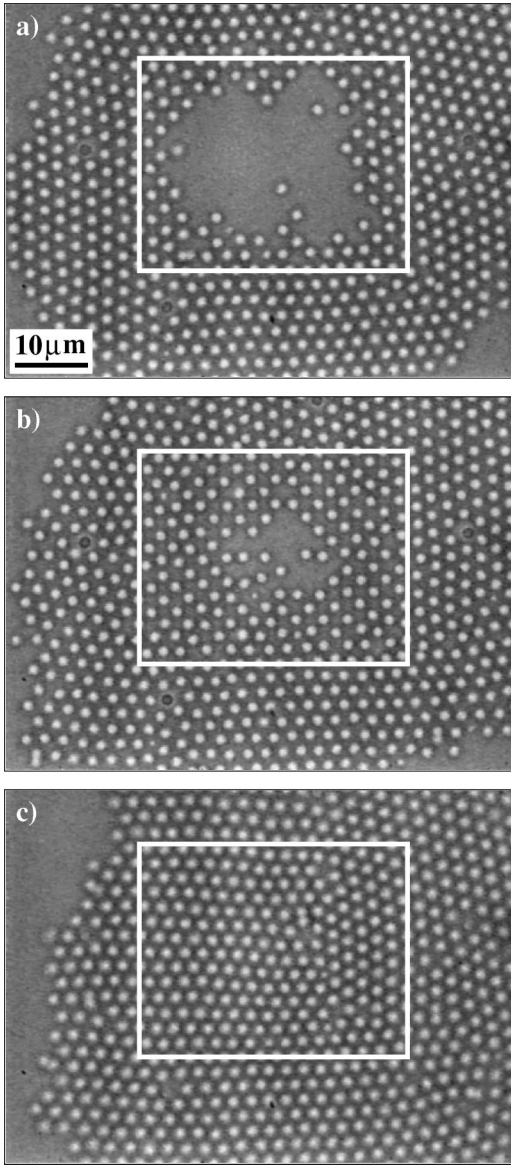


FIG. 2. Colloid invades the pinscape. (a)  $t=273$  sec after the tweezer array was activated, many spheres have assembled outside the pinscape. Spheres pinned at the edges block access to the interior, although some have penetrated by means of thermal hopping. (b)  $t=363$  sec: The array is mostly filled, through single-particle hopping and multiparticle avalanches. Spheres inside the pinscape exhibit fourfold order. (c)  $t=635$  sec: The particles have depinned and the monolayer has undergone a transition from fourfold to sixfold order. In all images, the white box indicates the region occupied by the tweezer array.

scape's static trapping potential. Rather than flowing continuously into the array of traps, most spheres remain pinned near the edge for long periods of time, as shown in Fig. 2(a). This kinetically hindered configuration closely resembles the critical state in type II superconductors.<sup>31,32</sup> In that state, magnetic flux lines become immobilized on defects in the superconductor and are forced by nearest neighbor and body forces to establish density gradients.

Spheres on the periphery of the trap array populate its interior via two distinct mechanisms: thermally activated

single-particle hopping and punctuated bursts of collective rearrangements reminiscent of avalanches in granular materials, vortex matter, and other jammed systems.<sup>33</sup> Although the individual spheres' diameters are smaller than the separation between optical tweezers, their electrostatic repulsion prevents them from filling every trap in the array. Hence, the spheres occupy every other lattice site, forming a  $\sqrt{2} \times \sqrt{2}$  superlattice rotated at  $45^\circ$  with respect to the trap array's axes. Figures 2(a) and 2(b) show the system in this state after 273 sec and 363 sec of illumination, respectively. Comparable superlattice structures have been observed for flux lines occupying square arrays of magnetic pinning centers patterned onto conventional superconductors.<sup>34</sup>

Once the superlattice is complete, subsequent filling causes the monolayer to depin from the trap array, at which point it undergoes a martensitic transition to a floating triangular crystal, as shown in Fig. 2(c). This final observation is somewhat surprising. If combined hydrodynamic and nearest-neighbor forces can depin individual spheres, why does the monolayer invade as a commensurate superlattice rather than as an incommensurate triangular array? While the particles' measured trajectories tell the whole story, three characteristics of their collective structure and cooperative motions highlight more generally relevant trends. In particular, we consider the local areal density  $\rho(t)$ , the particles' mean speed  $\langle v(t) \rangle$ , and the  $m$ -fold bond-orientational-order parameters<sup>1</sup> whose evolution in time appears in Fig. 3.

We measure the local areal density by calculating the area of each particle's nearest neighborhood or Wigner-Seitz cell.<sup>35</sup> These polygonal areas can be combined to define regional areal densities inside and outside the domain of the pinscape, as shown in Fig. 3(a). Spheres on the outer edge of the cluster, whose local density is not well defined, are not considered in computing the outer areal density. The outer areal density remains essentially constant even as spheres move into the pinscape and additional spheres arrive at the crystal's outer edges. This observation supports the conjecture that the toroidal flow establishes an effectively constant pressure at the monolayer's edges.

Like  $\rho(t)$ , the particles' mean speed  $\langle v(t) \rangle$  gauges the influx of spheres into the pinscape. It also captures local rearrangements that do not affect the density. Peaks in  $\langle v(t) \rangle$  are analogous to bursts of electrical activity observed in studies of superconducting vortex avalanches,<sup>36</sup> and indicate collective motion of a significant fraction of the particles inside the pinscape. Figure 3(b), shows the mean speed for particles within the pinscape averaged over 1 sec intervals.

To quantify how order evolves as spheres invade, we compute the local  $m$ -fold bond-orientational-order parameters<sup>1</sup>

$$\psi_m(\vec{r}_j) = \frac{1}{N_j} \sum_{k=1}^{N_j} \exp(im\theta_{jk}), \quad (3)$$

for  $m=6$  and  $8$ , where  $\vec{r}_j$  is the location of particle  $j$ , whose  $N_j$  nearest neighbors, labeled by  $k$ , are arrayed at angles  $\theta_{jk}$

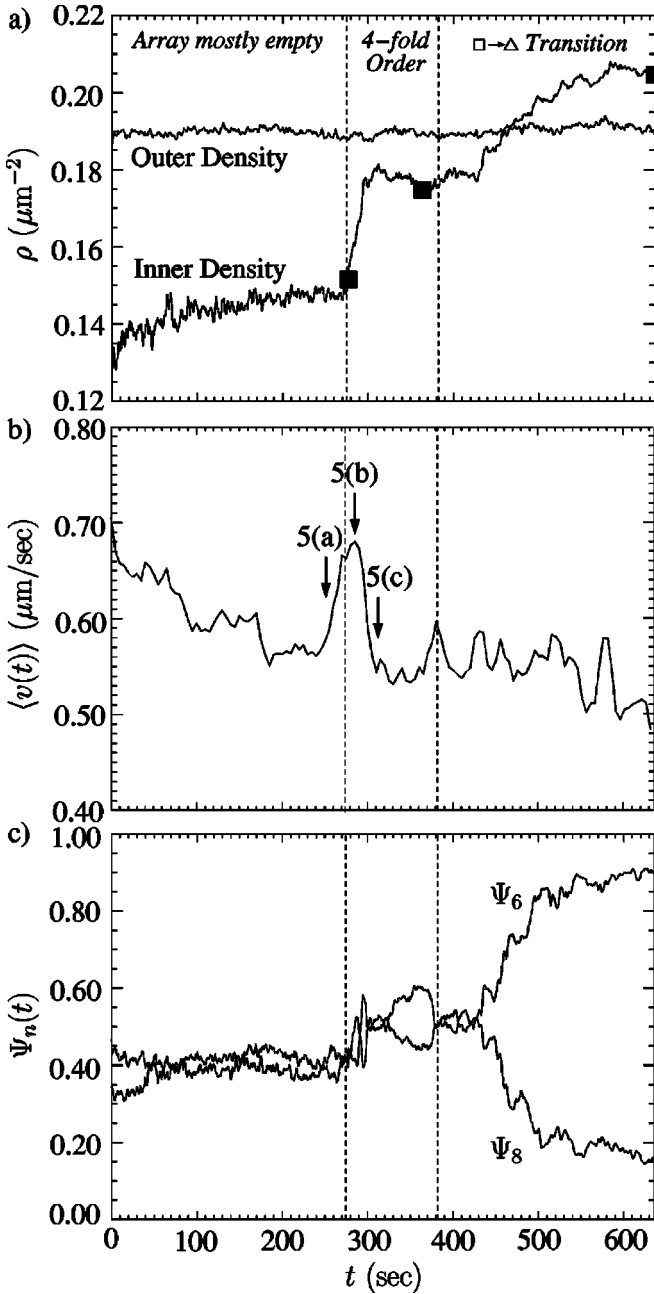


FIG. 3. (a) Areal density of spheres inside and outside the pinscape. Squares indicate times at which the images in Fig. 2 were obtained. (b) Average speed of particles within the pinscape over 1 sec intervals. Arrows near the primary avalanche indicate the periods over which the trajectory data in Fig. 5 were obtained. (c) Mean-square magnitudes of the six and eight fold bond-orientational order parameters for particles within the pinscape.

with respect to a reference axis. Each  $\psi_m(\vec{r}_j)$  achieves its maximum magnitude of unity if the neighborhood around particle  $j$  is perfectly  $m$  fold ordered. The mean-squared magnitude

$$\Psi_m(t) = \frac{1}{N(t)} \sum_{j=1}^{N(t)} |\psi_m[\vec{r}_j(t)]|^2 \quad (4)$$

for the  $N(t)$  particles within the pinscape's domain at time  $t$  measure the degree of  $m$ -fold order displayed by the system. While  $\Psi_6(t)$  measures sixfold order accurately,  $\Psi_8(t)$  is preferable to  $\Psi_4(t)$  for measuring fourfold order because of the former's ability to account for diagonal nearest-neighbor bonds in triangulations of square lattices. These order parameters appear in Fig. 3(c).

Taken together, the data in Fig. 3 reveal that the system's evolution proceeds in three phases. At first ( $0 < t < 276$  sec), the array fills slowly, as indicated by the gradually increasing inner density shown in Fig. 3(a). Nonetheless, the mean particle speed is high because of particles arriving at the pinscape's periphery from all sides. As these accessible sites become full, the spheres' inward motion becomes blocked and  $\langle v(t) \rangle$  decreases. During this period, the pinscape is mostly empty, so that  $\Psi_6(t)$  and  $\Psi_8(t)$  are consistent with a random distribution of points.

A large avalanche beginning at  $t=250$  sec initiates the invasion's second stage. Between  $t=276$  sec and  $t=300$  sec, the number of spheres inside the pinscape increases sharply. This is indicated by a sharp rise in  $\rho(t)$  and a corresponding peak in  $\langle v(t) \rangle$ . The sudden increase in density leads to a rapid growth in both  $\Psi_6(t)$  and  $\Psi_8(t)$ . Almost as soon as the avalanche ends, however,  $\Psi_6(t)$  declines while  $\Psi_8(t)$  continues to rise. The invading triangular crystal actually anneals into fourfold domains of the  $\sqrt{2} \times \sqrt{2}$  superlattice. This state is shown in Fig. 2(b). Even more surprising is the observation that the mean density within the pinscape actually decreases during this period.

Another avalanche at  $t=380$  sec ends the growth in fourfold order and ushers in the final phase of the invasion. As the density once again begins to increase, the monolayer disengages from the array of optical traps and reorganizes itself into a sixfold-ordered triangular crystal. This process requires collective rearrangements of particles as well as plastic and elastic distortion of the surrounding unpinned triangular crystal. From Fig. 3(b), we can see that these rearrangements occur through a series of avalanches, each signalled by a peak in  $\langle v(t) \rangle$ . The monolayer's evolution ends with the pinscape completely full of triangular crystal as shown in Fig. 2(c) so that no room is left for further incursions. The interior density eventually exceeds the outer density, presumably because of flow-induced body forces directing spheres inward.

Having used ensemble-averaged measures to establish the sequence of events by which spheres first occupy and then disengage from the optical trap array, we can seek explanations for these events in the microscopic trajectories of individual spheres. In particular, we would like to understand why spheres initially invade the pinscape as a  $\sqrt{2} \times \sqrt{2}$  superlattice if they reach equilibrium as a floating triangular crystal. Examining the particles' motion during the three phases of the invasion sheds light on the matter.

Particle trajectories<sup>20</sup> from the invasion's early phase reveal that spheres enter the array's interior by means of single-particle hops. Figure 4 shows the well-localized trajectories of 14 particles near the edge of the optical tweezer array obtained over 1 sec. Grid crossings in Fig. 4 indicate

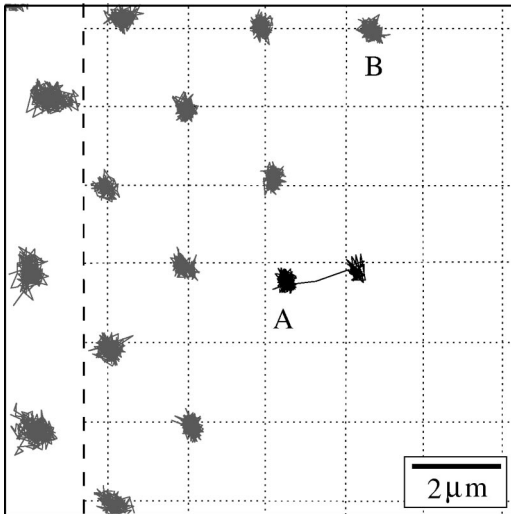


FIG. 4. Trajectories of individual colloidal particles localized in optical traps and in the crystal outside the trap array measured at  $\frac{1}{30}$ -sec intervals over 1 sec. Particle A can be seen hopping from a site misaligned with the  $\sqrt{2} \times \sqrt{2}$  domain to a commensurate site. The optical pinscape represented by crossings in the grid lines lies to the right of the dashed line.

individual traps' positions. Three particles to the left of the trap array are part of the unpinned crystalline reservoir and fluctuate about their equilibrium lattice positions more vigorously than do their neighbors pinned on optical traps. Of the pinned particles, only the ones labeled A and B are not centered on their tweezers. These two spheres are most closely associated with traps that are not part of the  $\sqrt{2} \times \sqrt{2}$  domain. If they were actually centered on these traps, the misfit spheres would be far closer to their neighbors than other spheres in the domain. Strong nearest-neighbor repulsions displace them from these minima. The barrier to hopping is thus reduced, and random thermal fluctuations eventually conspire with steady hydrodynamic drag to force sphere A into the nearest trap in the superlattice domain. Similar processes are observed in simulations of vortex dynamics in periodically pinned superconductors.<sup>37</sup>

Having observed individual spheres hopping preferentially onto optical tweezers at commensurate  $\sqrt{2} \times \sqrt{2}$  superlattice sites, we are in a position to explain the transient growth in  $\Psi_8(t)$  and the corresponding decrease in  $\rho(t)$  after the principal avalanche at  $t=280$  sec. Again, insight is gained by looking at the particle tracks. Figure 5 shows short trajectories over the entire field of view just before, during, and after this avalanche. Despite the initial increase in  $\langle v(t) \rangle$  at  $t=250$  sec, the pinned domain's density does not begin to increase until roughly 20 sec later. Figure 5(a) reveals that most particle motions in this early stage involve collective rearrangements in the surrounding triangular crystal, with only small streams of particles filing into the array. Streaming through pinning arrays also has been identified in simulations<sup>38,39</sup> and time-resolved imaging<sup>40</sup> of relaxation in the superconducting critical state.

The main part of the avalanche, shown in Fig. 5(b), involves highly cooperative translation of an entire triangular

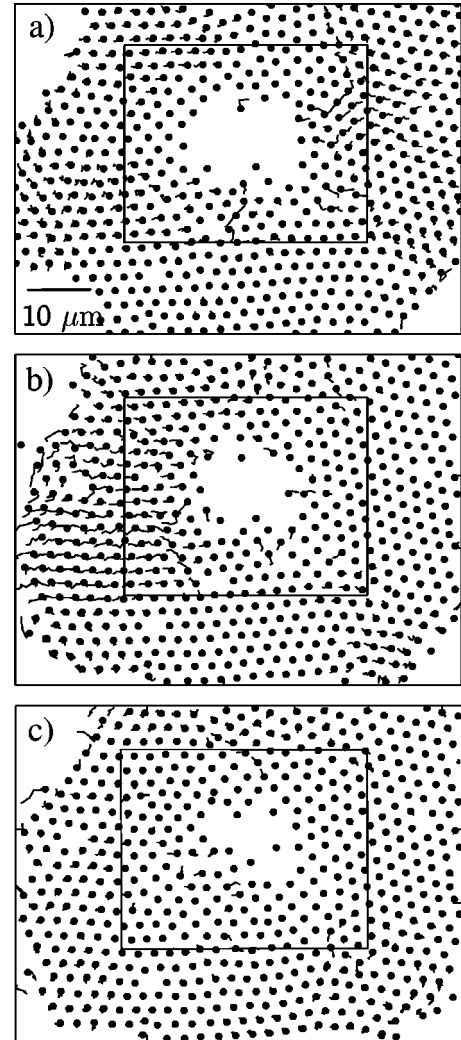


FIG. 5. Trajectories of colloidal particles over 3 sec intervals. Filled dots indicate the particles' final positions. Rectangles indicate the domain of the optical trap array. (a) Trajectories from the early stage of the principal avalanche. Most of the particles inside the pinscape are organized into fourfold domains. (b) The avalanche drives particles into the pinscape as a domain of sixfold order. (c) Fourfold order returns via single-particle hopping.

domain into the pinscape. Within 10 sec, however, most of the pinned crystal has recovered its fourfold superlattice structure, as shown in Fig. 5(c), largely through single-particle rearrangements of the kind shown in Fig. 4. Even if avalanches tend to force dense triangular crystal into the array, crowded spheres can advance into less dense and energetically more favorable superlattice configurations.

The resulting superlattice crystal consists of two incompatible domains. These compete for the pinscape by displacing spheres from their traps at the domain boundaries. Progress in domain coarsening involves pushing displaced spheres out of the pinned crystal and back into the surrounding reservoir of triangular crystal. This explains the transient decline in the pinned crystal's density after the avalanche.

Eventually, avalanches of spheres drive enough additional incommensurate crystal into the pinned domain's edges that the interior, now almost completely occupied, can no longer

accommodate further single-particle relaxation events. The advance of sixfold order then proceeds through local shearing rearrangements similar to those that characterize the one-layer to two-layer martensitic transition in colloid confined between parallel repulsive walls.<sup>41</sup> Locally shearing the square domains into triangular domains leads to the formation of misaligned triangular grains, as can be seen in Fig. 2(c). Once depinned, the incommensurate sixfold monolayer increases its density by annealing away the resulting grain boundaries, a very slow process involving rare cooperative motions of large numbers of spheres.

The same sequence of events was obtained reproducibly for separate runs of this experiment. The pattern of avalanches that first produces commensurate square superlattice coverages and eventually drives a symmetry-altering depinning transition proceeded in all cases through the same microscopic mechanisms observed for the particular run described above.

Qualitatively similar flux transport by hopping, streaming, and avalanches has been observed directly in thin superconducting films through Lorentz microscopy<sup>40</sup> and in microfabricated superconducting arrays by scanning probe microscopy.<sup>37</sup> Such mechanisms also have been inferred from transport measurements on conventional<sup>36,42</sup> and high-temperature superconductors. Order-order transitions similar to the one observed in this experiment have been inferred indirectly from transport measurements on patterned superconductors<sup>43–46</sup> and Josephson junction arrays.<sup>47</sup>

This study constitutes the demonstration of holographic optical tweezers' utility for studying cooperative phenomena in strongly coupled systems. As a model system, colloidal monolayers modulated by holographic optical tweezers offer the unique opportunity to both accurately measure and continuously control the particles' interactions with each other and with the substrate potential. Such control will make possible systematic studies of effects induced by varying the strength, scale, and symmetry of the pinning potential landscape, and could even allow for the study of the influence of controlled disorder deliberately encoded into the tweezer array. The laser-induced toroidal flow technique also introduced for this study is useful for establishing an essentially isotropic hydrostatic pressure on the pinned colloid. Still other insights can be gained by studying colloidal transport in linear flows. This work is ongoing and will be published elsewhere.

We are grateful to Heinrich Jaeger, Tom Witten, Franco Nori, and Charles Reichhardt for enlightening conversations. This work was supported in part by the MRSEC Program of the National Science Foundation through Grant No. DMR-980595, in part through NSF Grant No. DMR-978031, and in part by the David and Lucile Packard Foundation. Additional funding was provided by a grant from Arryx, Inc. The diffractive optical element used in this study was fabricated by Matthew Dearing and Steven Sheets to a design by Eric Dufresne using the methods of Ref. 18.

- 
- <sup>1</sup>C.A. Murray, in *Bond-Orientational Order in Condensed Matter Systems*, edited by K. J. Strandburg (Springer-Verlag, Berlin, 1991).
- <sup>2</sup>I. Lyuksyutov, A.G. Naumovets, and V. Pokrovsky, *Two-Dimensional Crystals* (Academic Press, San Diego, 1992).
- <sup>3</sup>V.V. Metlushko, M. Baert, R. Jonckheere, V.V. Moshchalkov, and Y. Bruynseraede, *Solid State Commun.* **91**, 331 (1994).
- <sup>4</sup>C. Reichhardt, C.J. Olson, and F. Nori, *Phys. Rev. B* **57**, 7937 (1998).
- <sup>5</sup>C.J. Olson, C. Reichhardt, and F. Nori, *Phys. Rev. Lett.* **81**, 3757 (1998).
- <sup>6</sup>C. Reichhardt and F. Nori, *Phys. Rev. Lett.* **82**, 414 (1999).
- <sup>7</sup>C. Reichhardt, R.T. Scalettar, G.T. Zimányi, and N. Grønbech-Jensen, *Phys. Rev. B* **61**, R11 914 (2000).
- <sup>8</sup>D.J. Morgan and J.B. Ketterson, *J. Low Temp. Phys.* **122**, 37 (2001).
- <sup>9</sup>*Intercalation in Layered Materials*, edited by M. S. S. Dresselhaus (Plenum Press, New York, 1986).
- <sup>10</sup>*Charge Density Waves in Solids*, edited by L.P. Gorkov and G. Grüner (North-Holland, New York, 1989).
- <sup>11</sup>A.D. Dinsmore, A.G. Yodh, and D.J. Pine, *Nature (London)* **383**, 239 (1996).
- <sup>12</sup>B.J. Ackerson and A.H. Chowdhury, *Faraday Discuss. Chem. Soc.* **83**, 1 (1987).
- <sup>13</sup>M.M. Burns, J.-M. Fournier, and J.A. Golovchenko, *Science* **249**, 749 (1990).
- <sup>14</sup>K. Loudiyi and B.J. Ackerson, *Physica A* **184**, 1 (1992).
- <sup>15</sup>Q.-H. Wei, C. Bechinger, D. Rudhardt, and P. Leiderer, *Phys. Rev. Lett.* **81**, 2606 (1998).
- <sup>16</sup>E.R. Dufresne and D.G. Grier, *Rev. Sci. Instrum.* **69**, 1974 (1998).
- <sup>17</sup>D. G. Grier and E. R. Dufresne, U.S. Patent No. 6,055,106 (2000).
- <sup>18</sup>E.R. Dufresne, G.C. Spalding, M.T. Dearing, S.A. Sheets, and D.G. Grier, *Rev. Sci. Instrum.* **72**, 1810 (2001).
- <sup>19</sup>A. Ashkin, J.M. Dziedzic, J.E. Bjorkholm, and S. Chu, *Opt. Lett.* **11**, 288 (1986).
- <sup>20</sup>J.C. Crocker and D.G. Grier, *J. Colloid Interface Sci.* **179**, 298 (1996).
- <sup>21</sup>S.H. Behrens and D.G. Grier, *Phys. Rev. E* **64**, 050401 (2001).
- <sup>22</sup>S.H. Behrens and D.G. Grier, *J. Chem. Phys.* **115**, 6716 (2001).
- <sup>23</sup>A.E. Larsen and D.G. Grier, *Phys. Rev. Lett.* **76**, 3862 (1996).
- <sup>24</sup>A.E. Larsen and D.G. Grier, *Nature (London)* **385**, 230 (1997).
- <sup>25</sup>G.M. Kepler and S. Fraden, *Phys. Rev. Lett.* **73**, 356 (1994).
- <sup>26</sup>J.C. Crocker and D.G. Grier, *Phys. Rev. Lett.* **77**, 1897 (1996).
- <sup>27</sup>M.D. Carbajal-Tinoco, F. Castro-Román, and J.L. Arauz-Lara, *Phys. Rev. E* **53**, 3745 (1996).
- <sup>28</sup>W.B. Russel, D.A. Saville, and W.R. Schowalter, *Colloidal Dispersions* (Cambridge University Press, Cambridge, 1989).
- <sup>29</sup>J. Happel and H. Brenner, *Low Reynolds Number Hydrodynamics* (Kluwer, Dordrecht, 1991).
- <sup>30</sup>J.C. Crocker and D.G. Grier, *Phys. Rev. Lett.* **73**, 352 (1994).
- <sup>31</sup>C.P. Bean, *Rev. Mod. Phys.* **36**, 31 (1964).
- <sup>32</sup>Y.B. Kim, C.F. Hempstead, and A.R. Strnad, *Rev. Mod. Phys.* **36**, 43 (1964).

- <sup>33</sup>A.J. Liu and S.R. Nagel, *Nature (London)* **396**, 21 (1998).
- <sup>34</sup>M.J. Van Bael, K. Temst, V.V. Moshchalkov, and Y. Bruynseraede, *Phys. Rev. B* **59**, 14 674 (1999).
- <sup>35</sup>F.P. Preparata and M.I. Shamos, *Computational Geometry* (Springer-Verlag, New York, 1985).
- <sup>36</sup>S. Field, J. Witt, F. Nori, and X. Ling, *Phys. Rev. Lett.* **74**, 1206 (1995).
- <sup>37</sup>C. Reichhardt, J. Groth, C.J. Olson, S.B. Field, and F. Nori, *Phys. Rev. B* **54**, 16 108 (1996).
- <sup>38</sup>F. Nori, *Science* **271**, 1373 (1996).
- <sup>39</sup>C.J. Olson, C. Reichhardt, and F. Nori, *Phys. Rev. Lett.* **80**, 2197 (1998).
- <sup>40</sup>K. Harada, O. Kamimura, H. Kasai, T. Matsuda, A. Tonomura, and V.V. Moshchalkov, *Science* **274**, 1167 (1996).
- <sup>41</sup>J.A. Weiss, D.W. Oxtoby, D.G. Grier, and C.A. Murray, *J. Chem. Phys.* **103**, 1180 (1995).
- <sup>42</sup>K. Behnia, C. Capan, D. Maily, and B. Etienne, *Phys. Rev. B* **61**, R3815 (2000).
- <sup>43</sup>V. Metlushko, U. Welp, G. W. Crabtree, R. Osgood, S. D. Bader, L. E. De Long, Z. Zhang, S. R. J. Brueck, B. Ilic, K. Chung, and P. J. Heaketh, *Phys. Rev. B* **60**, R12 585 (1999).
- <sup>44</sup>D.J. Morgan and J.B. Ketterson, *Phys. Rev. Lett.* **80**, 3614 (1998).
- <sup>45</sup>A. Terentiev, D. B. Watkins, L. E. De Long, L. D. Cooley, D. J. Morgan, and J. B. Ketterson, *Phys. Rev. B* **61**, R9249 (1999).
- <sup>46</sup>J.I. Martín, M. Vélez, A. Hoffmann, I.K. Schuller, and J.L. Vicent, *Phys. Rev. B* **62**, 9110 (2000).
- <sup>47</sup>V.I. Marconi and D. Domínguez, *Phys. Rev. Lett.* **82**, 4922 (1999).